

# Journal of Biomedical Optics

[SPIEDigitalLibrary.org/jbo](http://SPIEDigitalLibrary.org/jbo)

## **Investigating *in vivo* airway wall mechanics during tidal breathing with optical coherence tomography**

Claire Robertson  
Sang-Won Lee  
Yeh-Chan Ahn  
Sari Mahon  
Zhongping Chen  
Matthew Brenner  
Steven C. George

# Investigating *in vivo* airway wall mechanics during tidal breathing with optical coherence tomography

Claire Robertson,<sup>a,b</sup> Sang-Won Lee,<sup>c,d</sup> Yeh-Chan Ahn,<sup>c,e</sup> Sari Mahon,<sup>c</sup> Zhongping Chen,<sup>a,b,c</sup> Matthew Brenner,<sup>c,f</sup> and Steven C. George<sup>a,b,g</sup>

<sup>a</sup>University of California, Irvine, Department of Biomedical Engineering, Irvine, California 92697

<sup>b</sup>University of California, Irvine, The Edwards Lifesciences Center for Advanced Cardiovascular Technology, Irvine, California 92697

<sup>c</sup>University of California, Irvine, Beckman Laser Institute, 1002 Health Sciences Rd. East, Irvine, California 92612

<sup>d</sup>Electronics and Telecommunications Research Institute, 138 Gajeongno, Yuseong-gu, Daejeon 305-700, Korea

<sup>e</sup>Pukyong National University, Department of Biomedical Engineering, 599-1 Daeyeon 3-dong, Nam-gu, Busan, 608-737 Korea

<sup>f</sup>University of California Irvine Medical Center, Pulmonary and Critical Care Division, Orange, California 92868

<sup>g</sup>University of California, Irvine, Department of Chemical Engineering and Materials Science, Irvine, California 92697

**Abstract.** Optical coherence tomography (OCT) is a nondestructive imaging technique offering high temporal and spatial resolution, which makes it a natural choice for assessing tissue mechanical properties. We have developed methods to mechanically analyze the compliance of the rabbit trachea *in vivo* using tissue deformations induced by tidal breathing, offering a unique tool to assess the behavior of the airways during their normal function. Four-hundred images were acquired during tidal breathing with a custom-built endoscopic OCT system. The surface of the tissue was extracted from a set of these images via image processing algorithms, filtered with a bandpass filter set at respiration frequency to remove cardiac and probe motion, and compared to ventilatory pressure to calculate wall compliance. These algorithms were tested on elastic phantoms to establish reliability and reproducibility. The mean tracheal wall compliance (in five animals) was  $1.3 \pm 0.3 \times 10^{-5}$  (mm Pa)<sup>-1</sup>. Unlike previous work evaluating airway mechanics, this new method is applicable *in vivo*, noncontact, and loads the trachea in a physiological manner. The technique may have applications in assessing airway mechanics in diseases such as asthma that are characterized by significant airway remodeling. © 2011 Society of Photo-Optical Instrumentation Engineers (SPIE). [DOI: 10.1117/1.3642006]

Keywords: airway compliance; mechanics; *in vivo*; optical coherence tomography.

Paper 10666RRR received Dec. 18, 2010; revised manuscript received Aug. 5, 2011; accepted for publication Sep. 1, 2011; published online Oct. 14, 2011.

## 1 Introduction

Numerous lung diseases, such as asthma, may impact the mechanical behavior of the airway walls.<sup>1-3</sup> Airway remodeling, commonly observed in asthmatic patients, involves thickening of the mucosa, collagen deposition, and disruption of the normal elastin network, which can affect the tissue mechanics.<sup>4-9</sup> As airway smooth muscle contracts in parallel with the noncontractile tissue, changes in the mechanical properties of the tissue could affect smooth muscle contractility and thus the pathogenesis of asthma.<sup>3</sup> Assessing airway tissue mechanics *in vivo* could improve the understanding, diagnosis, and management of lung diseases such as asthma, which affect at least 5% of the U.S. adult population.<sup>10</sup>

The *in vivo* mechanical behavior of the airways remains poorly understood, as current techniques lack the temporal-spatial resolution necessary to track their deformation during normal tidal breathing. Current techniques to evaluate tissue compliance are either *ex vivo* techniques, which require excision and thus tissue disruption,<sup>11,12</sup> or *in vivo* techniques which either rely on contact with the tissue, loading the airways with nonphysiologic methods,<sup>2</sup> or rely on imaging methods which

lack the temporal resolution to measure deformations occurring within a single breath.<sup>13</sup> It is known that the smooth muscle surrounding the airways (the primary effector of airway narrowing in asthma) is acutely sensitive to strain and strain rate, suggesting that the ideal assessment of *in vivo* airway mechanics would be direct, noncontact measure of airway strain during normal, tidal breathing.

In order to track the small deformations occurring in the large airways during normal tidal breathing, an imaging modality with high spatial resolution (submillimeter), and high temporal resolution (>10 Hz) is needed. Optical coherence tomography (OCT) is an emerging medical imaging technique which allows for high resolution ( $\sim 10 \mu\text{m}/\text{pixel}$ ) images of tissue. Endoscopic probes have been developed for many organs, allowing imaging of the blood vessels, esophagus, urethra, and airways with a resolution previously only available via biopsy and histological preparation.<sup>14-21</sup> Recently developed Fourier-domain OCT techniques maintain the same spatial resolution while offering video-frame rates (up to 100 frames/s).<sup>20,21</sup> Furthermore, unlike ultrasound, OCT can be used in noncontact modes and in air-filled lumens, such as the airways. Thus, the speed and resolution of OCT make it potentially ideal for mechanical property assessment of the airways.<sup>22-31</sup>

Address all correspondence to: Steven George, University of California, Irvine, 2420 Engineering Hall, Irvine, California 92697. Tel: (949) 824-3941; Fax: (949) 824-9968; E-mail: scgeorge@uci.edu.

In order for OCT-based mechanical analysis of airways to be possible, algorithms adaptable to endoscopic probes are needed, as are ways to overcome confounding motion artifacts. One previous work took OCT images of the airways at end expiration with different levels of positive end expiratory pressure (PEEP), however this technique neither evaluated motion at respiration frequency nor was able to independently analyze different regions of the trachea.<sup>13</sup> While elastography methods which use cross correlation techniques have been published, these techniques are difficult to adapt to flexible probes.<sup>31</sup> Similarly, Doppler-based techniques are sensitive to probe motion as the tissue to be imaged and the endoscopic probe both move; thus, techniques which are robust to probe motion are needed.<sup>32,33</sup> We have developed a new algorithm for mechanical analysis of tissue using OCT *in vivo*, deemed OCT wall motion analysis (OCT-WMA). This approach offers a simple, robust estimate of the mechanical response of the airways to tidal breathing *in vivo*.

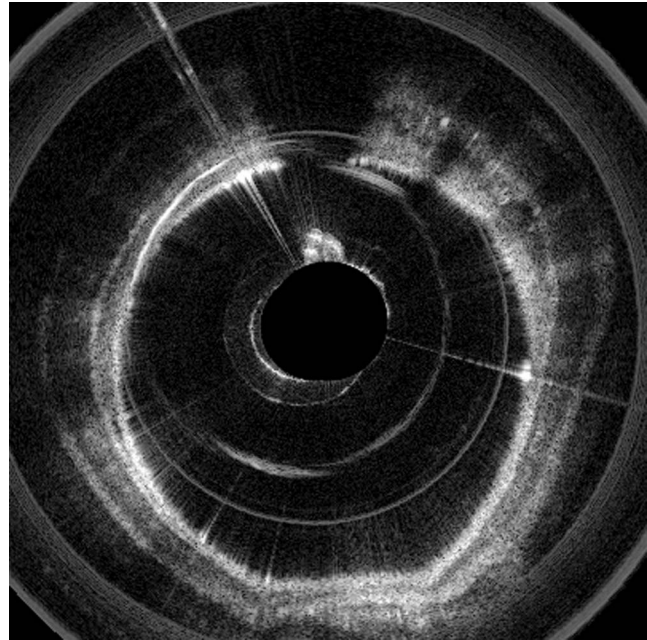
## 2 Methods

### 2.1 OCT System and Image Acquisition

The OCT system used for this study has been previously described.<sup>19,21</sup> OCT image stacks were acquired using a custom-built Fourier-domain system with an endoscopic probe, which was constructed with a rotating microelectromechanical motor (Namiki Prevision Jewel Co. Ltd., Tokyo, Japan), a single mode optical fiber gradient index lens (NSG America Inc., Somerset, New Jersey), and a 45° prism mirror (Tower Optical Corporation, Boynton Beach, Florida). This system uses a swept laser (Santec Corporation, Aichi, Japan) at 1310 nm with a full-width-half-maximum of 100 nm, giving a theoretical axial resolution of 7.5  $\mu\text{m}$ . The axial scan range was 3.5 mm in air and the sensitivity of this system was measured to be 107 dB with a 6-dB roll-off at the depth of 2.2 mm. The measured axial and lateral resolutions in air were 8 and 20  $\mu\text{m}$ , respectively. During tidal breathing, 400 two-dimensional (2D) images were taken of the same axial location with 1024 (lateral)  $\times$  400 (axial) pixel size at a rate of 19.5 frames/s (i.e., approximately 20 s of images of the same axial location) generating an image set for mechanical analysis (Video 1). Ventilatory pressure at the inlet and at the imaging site were measured concurrently with a 1 PSI transducer (Honeywell, Golden Valley, Minnesota) and a 1F catheter pressure transducer (Millar Instruments, Houston, Texas), respectively.

### 2.2 Algorithm Development

In order to calibrate distance in pixels from the OCT images and distance in millimeters, images were made in air of the inside of tubes of known radius, generating a linear ( $r^2 > 0.99$ ) calibration curve with a slope of 0.0103 mm/pixel in the radial direction. The surface of the tissue was identified in a semi-automated fashion via custom image processing scripts written in MATLAB (Mathworks, Natick, Massachusetts). As the swept-source OCT images used in this study contained a large number of artifacts due to internal reflections, specifying a search region in the image was necessary for accurate recognition of the tissue surface. Our algorithm has the user select 20 points along the surface in the first image of a 400-image set; then a curve is



**Video 1** This video shows the deformation of the *in vivo* rabbit trachea during normal ventilation. The trachealis can be seen at the bottom of the image. (MPEG, 63 KB) [URL: <http://dx.doi.org/10.1117/1.3642006.1>]

interpolated through these points via cubic splines. This spline curve serves to define the center of the search region, and the tissue surface in each vertical line is detected via a combination of gradient and intensity. The tissue surface in the first image slice then serves to define the search region in the next image of the set, and the process repeats through the entire 400-image set. By taking the surface of the tissue in each frame, the location of the tissue surface in space and time can be tracked. The repeatability of this algorithm was established via repeated (selecting a different set of initial 20 random points) analysis of the same image set. The average error between runs (with two different users) was 0.005 pixels/vertical scan line for six runs. In order to reduce the effect of probe motion, a circle was fit through the tissue surface in each image. The center of these circles was then co-localized and the surfaces adjusted accordingly.

As cardiac motion and other sources of noise generate unwanted deformations in the tissue, the next step in the analysis was to remove motion at frequencies other than the driving frequency of tidal breathing. At each radial location, respiratory motion was identified via a Fourier technique: the distance from probe center to tissue surface in time was extracted for each position around the trachea; then the Fourier transform of this data series was taken. The magnitude and phase of the peak at respiration frequency were extracted. This value is proportional to the peak-to-peak height of the motion due to respiration: If the series  $x_k$  is a discretized sinusoid, with amplitude  $A$  and period  $h/N$ , then the Fourier transform at frequency  $h$  is

$$F(h) = F(-h) = \sum_{n=0}^{N-1} \frac{A}{2} e^{(2\pi i/N)hn} e^{(-2\pi i/N)hn} = \frac{AN}{2}.$$

Therefore, to extract the amplitude at this frequency, we multiplied the discrete Fourier transform at the desired frequency

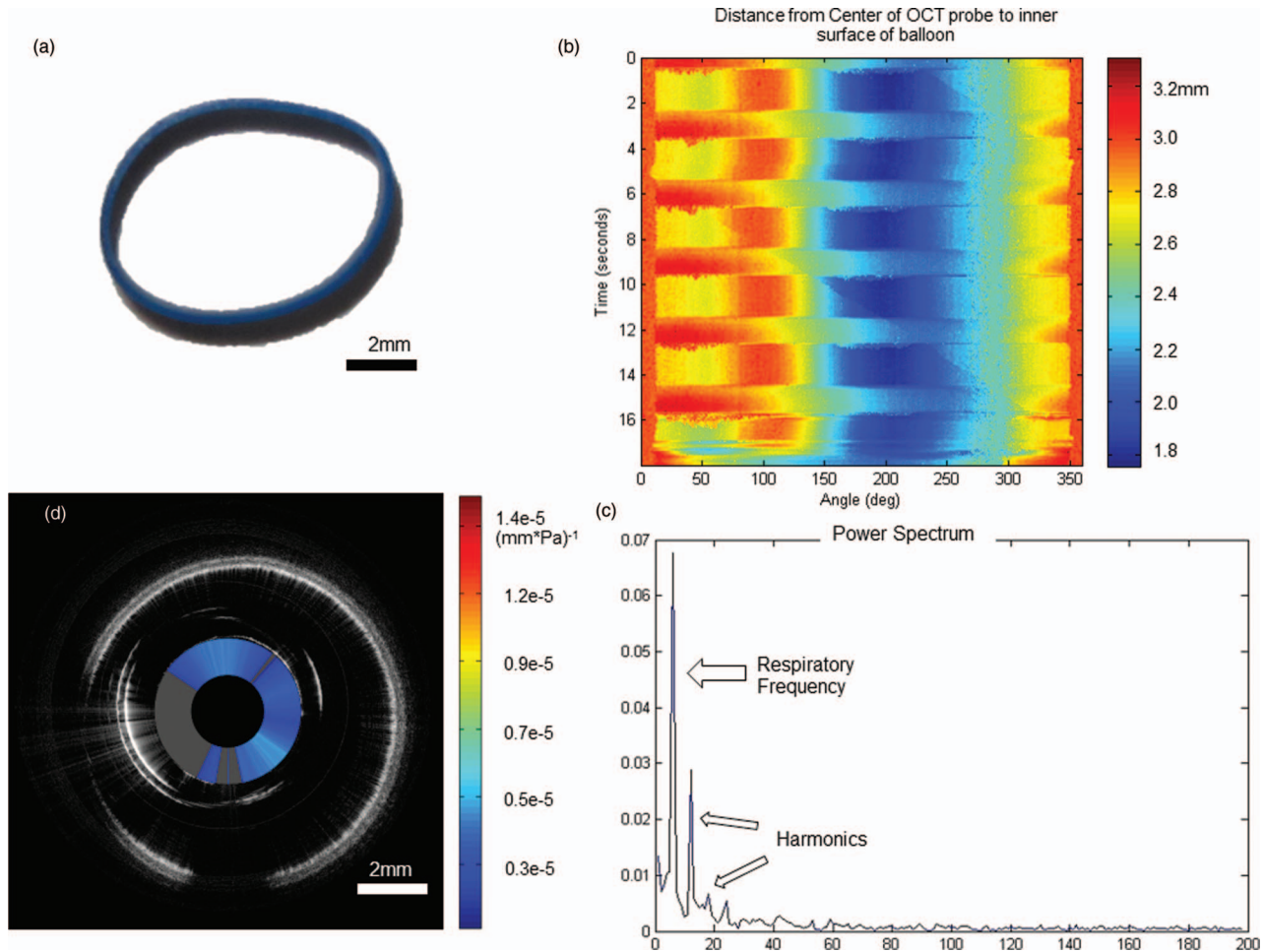


**Fig. 1** Analysis of an elastic phantom. (a) Photograph of the cross section of this flexible rubber tube. (b) The distance to the surface of the balloon from the center of the OCT probe (in millimeters). Note that the tube distends in time, as indicated by increased radius at certain times. (c) Shows the power spectrum of the average radius, demonstrating large peaks at respiration frequency and its harmonics. (d) Shows the OCT image of the tube itself with the compliance at any radial location given by the color of the disk in the center. Regions colored in gray were excluded from the analysis due to loss of useable signal.

by  $2/N$ . This value can be calculated for each angular position in the image, representing the peak-to-peak radial deformation in the tissue due to respiration at a given position in the trachea. The local radial deformation, measured by this technique, was then synced in time to a pressure tracing in order to give apparent local wall compliance. Radial strain ( $\varepsilon$ ) was defined as the change in the inner radius ( $\Delta r$ ) normalized to radius ( $r$ ) which is related to the change in the arc length ( $\Delta C$ ) of the trachea divided by the original arc length ( $C$ ):

$$\varepsilon = \frac{\Delta r}{r} = \frac{\Delta C}{C}. \quad (1)$$

The stress in the tracheal wall ( $\sigma$ ) times the thickness of the wall ( $d$ ) is equal to the pressure in the lumen ( $P$ ) times the radius.

$$\sigma \times d = P \times r. \quad (2)$$

The airway was then assumed to be a thin-walled tube, i.e., that the stress distribution inside the airway wall was homogeneous. These assumptions were chosen both as the mucosa is thin (micrometers) relative to the lumen of the airway (centimeters), and as the simplest model that could describe the inflation of a tube under pressure. While this assumption does

not recapitulate the complex anatomy of the airway wall and the undoubtedly complex stress field in it, it simplified the model to the point where a closed form analysis was possible.

Using the thin walled tube equation, Eqs. (1) and (2) can be rearranged to provide an expression for wall compliance,  $W_c$ .

$$W_c = \frac{\varepsilon}{\sigma \times d} = \frac{\Delta r/r}{P \times r} = \frac{1}{E \times d}. \quad (3)$$

As can be seen from Eq. (3),  $W_c$  is related to the inverse of the tangential modulus of the tissue ( $E$ ) and has units of  $(\text{mm Pa})^{-1}$ , allowing for comparison of the wall compliance calculated in this work and the more conventional tangential modulus.

### 3 Results

#### 3.1 Validation Using Phantoms

Our algorithm was validated by imaging and analyzing the material properties of elastic tube phantoms with both the proposed OCT WMA scheme and standard tensile mechanical testing. Two different phantoms were created, a uniform elastic tube and a tube with different compliances in the circumferential direction. First, the uniform tube-shaped elastic phantom was inflated

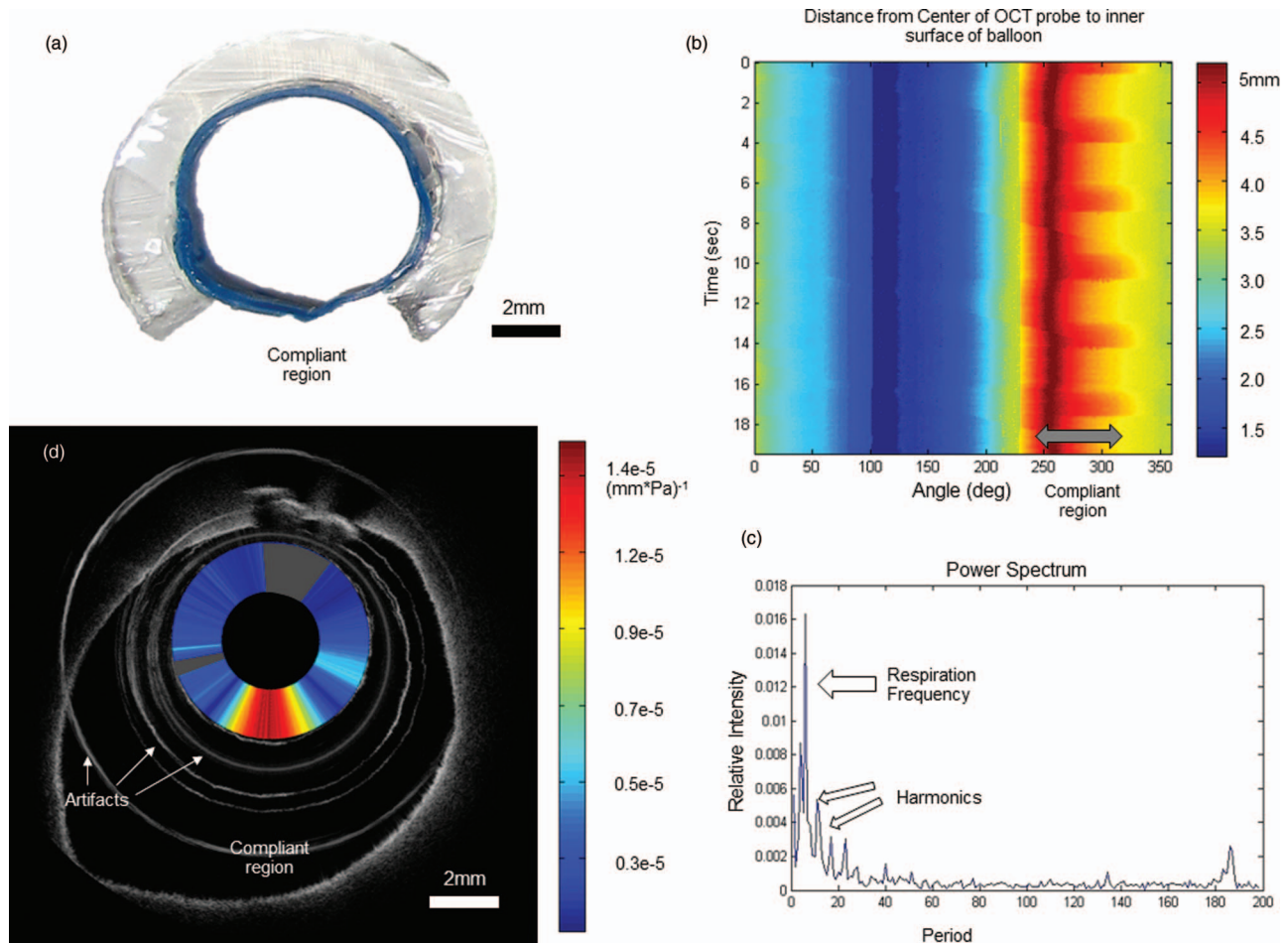


**Fig. 2** Analysis of the second phantom, in which circumferential regions have different compliances. (a) A cross section of this phantom made from rigid PVC tubing (clear) and a compliant elastic portion. (b) The distance to the surface of this phantom from the center of the OCT probe in time. Note that motion is confined to a specific circumferential section of the surface, indicated by the blue arrows corresponding to the absence of the rigid outer tube. (c) The power spectrum, where again, a large peak at respiration frequency can be seen. (d) The OCT image of this phantom, plus the compliance color map in the polar domain. Note that with OCT the different layers cannot be discerned; however, the compliance map indicates the region in which the stiff outer tubing is absent.

using a small animal ventilator (Harvard Apparatus, Holliston, Massachusetts) during imaging, while the ventilatory pressure was recorded using a 12bit A/D system (I-158, DATAQ, Akron, Ohio) with a calibrated 1 psi transducer at the inlet (Honeywell, Morristown, New Jersey) and a 1F catheter pressure transducer at the imaging site (Millar Instruments, Houston, Texas). The same material was then cut into 6-mm wide  $\times$  2-cm long strips and tested in tensile loading from 0 to 78 kPa of stress (equivalent to the stress range during tidal inflation) at a strain rate of 1 mm/min on a uniaxial test frame (MTS Synergie 100, MTS, Eden Prairie, Minnesota). Materials testing of the phantom (tangential modulus-  $1.3 \pm 0.3$  MPa) gives a  $W_c$  of  $6.0 \pm 1.3 \times 10^{-6}$  (mm Pa) $^{-1}$ . The wall compliance calculated from OCT imaging was  $4.5 \pm 2 \times 10^{-6}$  mm Pa $^{-1}$  if using the pressure sensor at the inlet and  $6.3 \pm 0.3 \times 10^{-6}$  mm Pa $^{-1}$  if using the sensor at the imaging site (Fig. 1). Next, we tested our algorithm in a phantom with a rigid (thick PVC tubing) and a compliant section (thin rubber) to model the trachea (rigid C-shaped cartilage rings attached by the compliant trachealis muscle). We were readily able to discern the compliant section via these methods, even though we could not directly image the rigid tubing from these images (Fig. 2).

### 3.2 *In Vivo* Wall Motion Analysis of Rabbit Trachea

Mechanical analysis using OCT was performed *in vivo* in a rabbit model. The animals (male adult New Zealand White, 4 to 4.5 kg, Western Oregon Rabbit Co. Philomath, Oregon) were anesthetized with a ketamine-xylazine mixture, intubated with a 3.5 mm endotracheal tube, and imaged with our OCT system as described above and previously.<sup>11,15,16</sup> All methods were approved by the Institutional Animal Care and Use Committee at the University of California, Irvine (Protocol No. 2007-2754). The OCT probe was inserted into the trachea of the animal through the intubation tube, and the tip positioned approximately 1 cm beyond the distal end of the intubation tube within the lower trachea. An image set was acquired (as described in Sec. 2.2) while the animal was ventilated during normal tidal breathing (Video 1). The image set was processed as described above in order to suppress motion artifacts (e.g., probe motion, cardiac motion) and calculate local wall compliance (Fig. 3) By stacking images at different axial locations along the trachea, a compliance map of the trachea can be generated (Fig. 4). The mean tracheal stiffness across polar coordinate and longitudinal distance was approximately  $1.3 \pm 0.3 \times 10^{-5}$  mm Pa $^{-1}$ . This value gives a tangential modulus of 25 to 75 kPa (assuming a range of tissue thickness

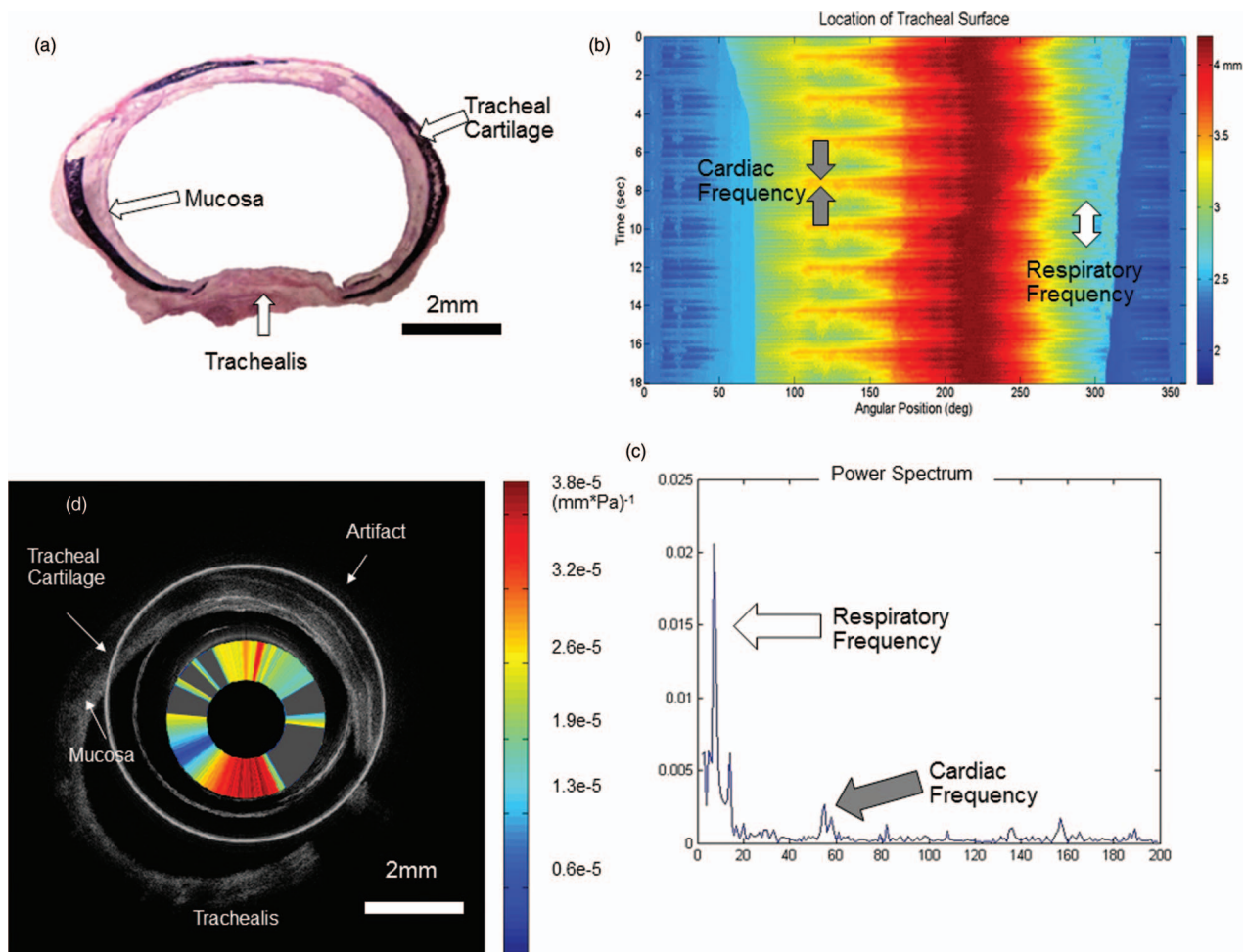


**Fig. 3** Analysis of rabbit trachea *in vivo*. (a) Hematoxylin and Eosin (H&E) staining of the rabbit trachea in cross section, where tracheal cartilage and the trachealis muscle can be seen. (b) The distance to the surface of the tissue from the center of the OCT probe. Note that both respiration and cardiac motion contribute to generate two overlapped sinusoids (indicated by white and gray arrows, respectively). In (c) the power spectrum from motion due to respiration is the notable peak at low frequency (white arrow), and the smaller peak represents cardiac frequency (gray arrow). (d) An OCT cross section of the trachea with the color map of compliance. Note that the trachealis (and thus absence of cartilage) corresponds to the most compliant region.

of 1 to 3 mm) which differs appreciably from the previously reported *ex vivo* modulus of 4.1 kPa.<sup>11</sup> Increased compliance is notable in the region corresponding to the trachealis, and closer to the carina.

#### 4 Discussion

Evaluating the mechanical properties of the airways during normal ventilatory function may aid in the understanding of pulmonary diseases ranging from asthma to sleep apnea; however, previous methods have not been able to capture *in vivo* airway mechanical behavior with normal breathing generating the displacements. Using OCT to image the airway wall, we have developed algorithms to extract airway wall motion during normal, tidal ventilation, calculate wall compliance, validated these techniques against phantoms, and used them to calculate wall compliance *in vivo*. Since OCT has higher spatial and temporal resolution than previously used techniques such as ultrasound or magnetic resonance, this technique presents a potential advance for *in vivo* analysis of tissue mechanics. This technique is distinct from previously described elastography algorithms, as it tracks the surface of the tissue in time, as opposed to

using cross correlation to track movement within the tissue.<sup>23,24,34</sup> This offers improved signal-to-noise, but loses the ability to track different tissue layers.

Unlike previous works which investigated tissue mechanics by measuring relative strain,<sup>35,36</sup> we directly measured both strain and driving pressure, allowing for quantitative analysis of the airway wall mechanics and comparison to other mechanical testing methods. Additionally, we have demonstrated techniques which function at breathing frequency and localize motion to different regions of the trachea: significant advances compared to previous *in vivo* work.<sup>13</sup> Validation with phantoms showed good accordance between the methods developed in this work and standard mechanical testing. A tissue thickness range of 1 to 3 mm [Eq. (3)], our value for  $W_c$  gives a tangential modulus of approximately 25 to 75 kPa, which is larger than the previously reported *ex vivo* modulus of 4.1 kPa.<sup>11</sup> This difference may be due to active smooth muscle tension during normal loading *in vivo*.<sup>37</sup>

This technique does have limitations. The probe size is large relative to the lumen diameter of the endotracheal tube, which could distort the air flow pattern; however, we have

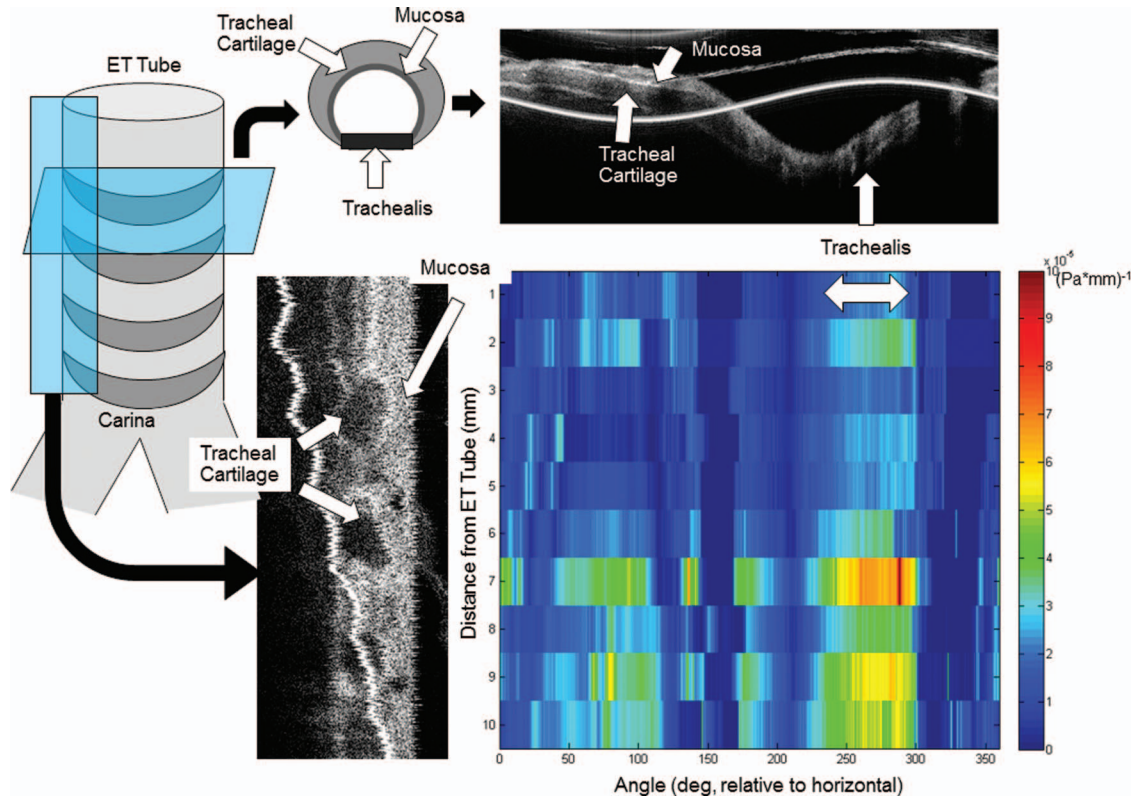


**Fig. 4** An *in vivo* map of tracheal compliance. By analyzing different axial positions between the end of the endotracheal (ET) tube and the carina, a 2D map of compliance was generated. The top portion of the compliance map is 1 mm distal to the ET tube, and the bottom portion is 10 mm distal. Angle refers to angle from horizontal, with the trachealis at 270 deg (indicated by white arrows). Structural OCT images, both axial (top) and longitudinal (side) are shown for comparison. In these images, features such as the mucosal thickness and the tracheal cartilage can be seen.

attempted to mitigate these effects by measuring the pressure at the imaging site. Similarly, given the size of our OCT probe we could not image smaller airways in a rabbit model, though the size of the probe would allow imaging of human airways down to generation #5 (diameter > 3 mm).<sup>38</sup> Additionally, the technique developed in this work calculates compliance based on radial deformation, ignoring deformations in the circumferential direction. It is possible that in inhomogeneous materials we miss some purely circumferential deformation even though increases in circumference are linked to increases in radius [by Eq. (1)]. Finally, the deformations of the wall surface represent a composite for all the tissue under the surface; thus, our technique cannot assess the mechanical properties of specific tissue layers (e.g., smooth muscle alone). Furthermore, for the analysis of relative compliance, the stress in the wall was considered to be homogeneous (thin wall assumption), which is not an accurate representation of the unknown (but undoubtedly complex) stress distribution in the wall. This assumption was used as the thickness of the airway wall cannot be directly measured from the OCT images (as the distance in pixels depends on the index of refraction of the mucosa—currently unknown) and to simplify the mathematics to an easily understood and simply computed model. These assumptions undoubtedly oversimplify the problem; however, they reduce an essentially unsolvable system to interesting metrics of strain in various regions of the tissue.

Unlike previous techniques, our algorithm considers dynamic changes in driving pressure instead of measuring only relative image strain. Even though our method is simpler than

many previously suggested algorithms, it remains robust to noise. Several previous reports have used cross correlation-based techniques to investigate tissue mechanics;<sup>22,23,25–27,39,40</sup> however, we found that with probe and cardiac motion accounting for as much as 50% of the observed deformation, alternative techniques were needed. Similarly, Doppler-based techniques work best when unwanted motion is considerably slower and of smaller magnitude than the deformation of interest. For example, blood flow is easily quantified this way.<sup>41,42</sup> In contrast, the cardiac motion artifact from this study was faster and of similar magnitude to the respiratory motion, yet our technique of Fourier transform and bandpass filtering was able to reject this unwanted motion artifact without compromising accuracy.

## 5 Conclusions

We have developed a new OCT-based method to analyze the mechanical properties of airways. By comparing the deflection of the surface of the tissue to ventilatory pressure during tidal breathing we have evaluated *in vivo* mechanical behavior (i.e., wall compliance) of a rabbit trachea. The high temporal and spatial resolution of OCT makes this technique more sensitive than previously reported techniques, and concurrent pressure monitoring allows for the estimation of the absolute compliance. This technique may have applications in research and clinical diagnostics and may facilitate our understanding of *in vivo*

airway dynamics of prevalent lung diseases such as asthma that are characterized by change in tissue mechanics.

### Acknowledgments

We would like to thank David Mukai, Tanya Burney, David Yoon, Kenji Ikemura, Emerald Chun, and Anna Aledia for their contributions. We would also like to acknowledge our funding sources including NIH 5R01CA124967 and NIH R01HL067954. Claire Robertson is supported by the NSF Graduate Research Fellowship Program.

### References

- N. J. Brown, C. M. Salome, N. Berend, C. W. Thorpe, and G. G. King, "Airway distensibility in adults with asthma and healthy adults, measured by forced oscillation technique," *Am. J. Respir. Crit. Care Med.* **176**(2), 129–137 (2007).
- H. J. Brackel, O. F. Pedersen, P. G. Mulder, S. E. Overbeek, K. F. Kerrebijn, and J. M. Bogaard, "Central airways behave more stiffly during forced expiration in patients with asthma," *Am. J. Respir. Crit. Care Med.* **162**(3 Pt 1), 896–904 (2000).
- A. M. Bramley, R. J. Thomson, C. R. Roberts, and R. R. Schellenberg, "Hypothesis: excessive bronchoconstriction in asthma is due to decreased airway elastance," *Eur. Respir. J.* **7**(2), 337–341 (1994).
- Y. Bosse, P. D. Pare, and C. Y. Seow, "Airway wall remodeling in asthma: from the epithelial layer to the adventitia," *Curr. Allergy Asthma Rep.* **8**(4), 357–366 (2008).
- W. Busse, J. Elias, D. Sheppard, and S. Banks-Schlegel, "Airway remodeling and repair," *Am. J. Respir. Crit. Care Med.* **160**(3), 1035–1042 (1999).
- F. H. Chen, K. T. Samson, K. Miura, K. Ueno, Y. Odajima, T. Shougo, Y. Yoshitsugu, and S. Shioda, "Airway remodeling: a comparison between fatal and nonfatal asthma," *J. Asthma* **41**(6), 631–638 (2004).
- J. A. Elias, "Airway remodeling in asthma. Unanswered questions," *Am. J. Respir. Crit. Care Med.* **161**(3 Pt 2), S168–S171 (2000).
- J. A. Elias, Z. Zhu, G. Chupp, and R. J. Homer, "Airway remodeling in asthma," *J. Clin. Invest.* **104**(8), 1001–1006 (1999).
- B. Fabry and J. J. Fredberg, "Remodeling of the airway smooth muscle cell: are we built of glass?" *Respir. Physiol. Neurobiol.* **137**(2–3), 109–124 (2003).
- T. M. Eagan, J. C. Brogger, G. E. Eide, and P. S. Bakke, "The incidence of adult asthma: a review," *Int. J. Tuberc. Lung Dis.* **9**(6), 603–612 (2005).
- C. B. Raub, S. Mahon, N. Narula, B. J. Tromberg, M. Brenner, and S. C. George, "Linking optics and mechanics in an *in vivo* model of airway fibrosis and epithelial injury," *J. Biomed. Opt.* **15**(1), 015004.
- P. R. Cooper, B. E. McParland, H. W. Mitchell, P. B. Noble, A. Z. Politi, A. R. Ressmeyer, and A. R. West, "Airway mechanics and methods used to visualize smooth muscle dynamics *in vitro*," *Pulm. Pharmacol. Ther.* **22**(5), 398–406 (2009).
- J. P. Williamson, R. A. McLaughlin, W. J. Noffsinger, A. L. James, V. A. Baker, A. Curatolo, J. J. Armstrong, A. Regli, K. L. Shepherd, G. B. Marks, D. D. Sampson, D. R. Hillman, and P. R. Eastwood, "Elastic properties of the central airways in obstructive lung diseases measured using anatomical optical coherence tomography," *Am. J. Respir. Crit. Care Med.* **183**, 612–619 (2011).
- J. Armstrong, M. Leigh, I. Walton, A. Zvyagin, S. Alexandrov, S. Schwer, D. Sampson, D. Hillman, and P. Eastwood, "In *in vivo* size and shape measurement of the human upper airway using endoscopic longrange optical coherence tomography," *Opt. Express* **11**(15), 1817–1826 (2003).
- M. Brenner, K. Kreuter, J. Ju, S. Mahon, L. Tseng, D. Mukai, T. Burney, S. Guo, J. Su, A. Tran, A. Batchinsky, L. C. Cancio, N. Narula, and Z. Chen, "In *in vivo* optical coherence tomography detection of differences in regional large airway smoke inhalation induced injury in a rabbit model," *J. Biomed. Opt.* **13**(3), 034001 (2008).
- M. Brenner, K. Kreuter, D. Mukai, T. Burney, S. Guo, J. Su, S. Mahon, A. Tran, L. Tseng, J. Ju, and Z. Chen, "Detection of acute smoke-induced airway injury in a New Zealand white rabbit model using optical coherence tomography," *J. Biomed. Opt.* **12**(5), 051701 (2007).
- S. Han, N. H. El-Abbadi, N. Hanna, U. Mahmood, R. Mina-Araghi, W. G. Jung, Z. Chen, H. Colt, and M. Brenner, "Evaluation of tracheal imaging by optical coherence tomography," *Respiration* **72**(5), 537–541 (2005).
- N. Hanna, D. Saltzman, D. Mukai, Z. Chen, S. Sasse, J. Milliken, S. Guo, W. Jung, H. Colt, and M. Brenner, "Two-dimensional and 3-dimensional optical coherence tomographic imaging of the airway, lung, and pleura," *J. Thorac. Cardiovasc. Surg.* **129**(3), 615–622 (2005).
- J. Su, J. Zhang, L. Yu, G. C. H. M. Brenner, and Z. Chen, "Real-time swept source optical coherence tomography imaging of the human airway using a microelectromechanical system endoscope and digital signal processor," *J. Biomed. Opt.* **13**(3), 030506 (2008).
- T. Xie, G. Liu, K. Kreuter, S. Mahon, H. Colt, D. Mukai, G. M. Peavy, Z. Chen, and M. Brenner, "In *in vivo* three-dimensional imaging of normal tissue and tumors in the rabbit pleural cavity using endoscopic swept source optical coherence tomography with thoracoscopic guidance," *J. Biomed. Opt.* **14**(6), 064045 (2009).
- J. Yin, G. Liu, J. Zhang, L. Yu, S. Mahon, D. Mukai, M. Brenner, and Z. Chen, "In *in vivo* early detection of smoke-induced airway injury using three-dimensional swept-source optical coherence tomography," *J. Biomed. Opt.* **14**(6), 060503 (2009).
- S. G. Adie, B. F. Kennedy, J. J. Armstrong, S. A. Alexandrov, and D. D. Sampson, "Audio frequency *in vivo* optical coherence elastography," *Phys. Med. Biol.* **54**(10), 3129–3139 (2009).
- R. Chan, A. Chau, W. Karl, S. Nadkarni, A. Khalil, N. Iftimia, M. Shishkov, G. Tearney, M. Kaazempur-Mofrad, and B. Bouma, "OCT-based arterial elastography: robust estimation exploiting tissue biomechanics," *Opt. Express* **12**(19), 4558–4572 (2004).
- B. F. Kennedy, T. R. Hillman, R. A. McLaughlin, B. C. Quirk, and D. D. Sampson, "In *in vivo* dynamic optical coherence elastography using a ring actuator," *Opt. Express* **17**(24), 21762–21772 (2009).
- A. S. Khalil, R. C. Chan, A. H. Chau, B. E. Bouma, and M. R. Mofrad, "Tissue elasticity estimation with optical coherence elastography: toward mechanical characterization of *in vivo* soft tissue," *Ann. Biomed. Eng.* **33**(11), 1631–1639 (2005).
- S. J. Kirkpatrick, R. K. Wang, and D. D. Duncan, "OCT-based elastography for large and small deformations," *Opt. Express* **14**(24), 11585–11597 (2006).
- H. J. Ko, W. Tan, R. Stack, and S. A. Boppart, "Optical coherence elastography of engineered and developing tissue," *Tissue Eng.* **12**(1), 63–73 (2006).
- X. Liang and S. Boppart, "Biomechanical properties of *in vivo* human skin from dynamic optical coherence elastography," *IEEE Trans. Biomed. Eng.* **57**(4), 953–959 (2009).
- J. Rogowska, N. A. Patel, J. G. Fujimoto, and M. E. Brezinski, "Optical coherence tomographic elastography technique for measuring deformation and strain of atherosclerotic tissues," *Heart* **90**(5), 556–562 (2004).
- J. Schmitt, "OCT elastography: imaging microscopic deformation and strain of tissue," *Opt. Express* **3**(6), 199–211 (1998).
- G. van Soest, F. Mastik, N. de Jong, and A. F. van der Steen, "Robust intravascular optical coherence elastography by line correlations," *Phys. Med. Biol.* **52**(9), 2445–2458 (2007).
- J. Walther, A. Kruger, M. Cuevas, and E. Koch, "Effects of axial, transverse, and oblique sample motion in FD OCT in systems with global or rolling shutter line detector," *J. Opt. Soc. Am. A* **25**(11), 2791–2802 (2008).
- Z. Xu, L. Carrion, and R. Maciejko, "A zero-crossing detection method applied to Doppler OCT," *Opt. Express* **16**(7), 4394–4412 (2008).
- R. Karimi, T. Zhu, B. E. Bouma, and M. R. Mofrad, "Estimation of nonlinear mechanical properties of vascular tissues via elastography," *Cardiovasc. Eng.* **8**(4), 191–202 (2008).
- E. I. Cespedes, C. L. de Korte, and A. F. van der Steen, "Intraluminal ultrasonic palpation: assessment of local and cross-sectional tissue stiffness," *Ultrasound Med. Biol.* **26**(3), 385–396 (2000).
- M. M. Doyley, F. Mastik, C. L. de Korte, S. G. Carlier, E. I. Cespedes, P. W. Serruys, N. Bom, and A. F. van der Steen, "Advancing intravascular ultrasonic palpation toward clinical applications," *Ultrasound Med. Biol.* **27**(11), 1471–1480 (2001).
- S. S. An, T. R. Bai, J. H. Bates, J. L. Black, R. H. Brown, et al., "Airway smooth muscle dynamics: a common pathway of airway obstruction in asthma," *Eur. Respir. J.* **29**(5), 834–860 (2007).

38. E. R. Weibel, "Morphometry of the human lung: the state of the art after two decades," *Bull. Eur. Physiopathol. Respir.* **15**(5), 999–1013 (1979).
39. R. A. Baldewsing, J. A. Schaar, F. Mastik, and A. F. van der Steen, "Local elasticity imaging of vulnerable atherosclerotic coronary plaques," *Adv. Cardiol.* **44**, 35–61 (2007).
40. Y. Li and J. G. Snedeker, "Elastography: modality-specific approaches, clinical applications, and research horizons," *Skeletal. Radiol.* **40**(4), 389–397 (2011).
41. A. Davis, J. Izatt, and F. Rothenberg, "Quantitative measurement of blood flow dynamics in embryonic vasculature using spectral Doppler velocimetry," *Anat. Rec.* **292**(3), 311–319 (2009).
42. A. Mariampillai, B. A. Standish, E. H. Moriyama, M. Khurana, N. R. Munce, M. K. Leung, J. Jiang, A. Cable, B. C. Wilson, I. A. Vitkin, and V. X. Yang, "Speckle variance detection of microvasculature using swept-source optical coherence tomography," *Opt. Lett.* **33**(13), 1530–1532 (2008).